



1 Identification of secondary aerosol precursors emitted by an 2 aircraft turbofan

3 Dogushan Kilic¹, Imad El Haddad¹, Benjamin T. Brem^{2,5}, Emily Bruns¹, Carlo Bozetti¹, Joel
4 Corbin¹, Lukas Durdina^{2,5}, Ru-Jin Huang¹, Jianhui Jiang¹, Felix Klein¹, Avi Lavi⁴, Simone M.
5 Pieber¹, Theo Rindlisbacher³, Yinon Rudich⁴, Jay G. Slowik¹, Jing Wang^{2,5}, Urs
6 Baltensperger¹, and Andre S. H. Prévôt¹

7 ¹Laboratory of Atmospheric Chemistry, Paul Scherrer Institute, Villigen PSI, 5400, Switzerland

8 ²Laboratory for Advanced Analytical Technologies, Empa, Dübendorf, 8600, Switzerland

9 ³Federal Office of Civil Aviation, Bern, 3003, Switzerland

10 ⁴Department of Earth and Planetary Sciences, Weizmann Institute of Science - Rehovot – Israel

11 ⁵Institute of Environmental Engineering, ETH Zurich, Zurich, 8093, Switzerland

12 Correspondence to: andre.prevot@psi.ch and imad.el-haddad@psi.ch

13 **Abstract.** Oxidative processing of aircraft turbine-engine exhaust was studied using a potential aerosol mass
14 (PAM) chamber at different engine loads corresponding to typical flight operations. Measurements were
15 conducted at an engine test cell. Organic gases (OGs) and particle emissions pre/post PAM were measured. A
16 suite of instruments, including a proton-transfer-reaction mass spectrometer (PTR-MS) for OGs, a multi-gas
17 analyzer for CO, CO₂, NO_x, and an aerosol mass spectrometer (AMS) for non-refractory particulate matter (NR-
18 PM₁) were used. Total aerosol mass was dominated by secondary aerosol formation, which was approximately
19 two orders of magnitude higher than the primary aerosol. The chemical composition of both gaseous and
20 particle emissions were also monitored at different engine loads and were thrust dependent. At idling load
21 (thrust 2.5-7%), more than 90% of the secondary particle mass was organic and could be explained by the
22 oxidation of gaseous aromatic species/OGs; *e.g.* benzene, toluene, xylenes, tri-, tetra-, and pentamethyl-benzene
23 and naphthalene. The oxygenated-aromatics, *e.g.* phenol, furans, were also included in this aromatic fraction and
24 their oxidation could alone explain up to 25% of the secondary organic particle mass at idling loads. The organic
25 fraction decreased with thrust level, while the inorganic fraction increased. At an approximated cruise load
26 sulfates comprised 85% of the total secondary particle mass.

27 1 Introduction

28 Airport activities emit both particulate and gaseous emissions (Unal et al., 2005; Hudda et al., 2014), and are a
29 significant source of local gas- and particle-phase pollutants (Westerdahl et al., 2008). These emissions affect
30 public health (Lin et al., 2008) and local air quality by increasing pollutant concentrations, *e.g.* ultrafine
31 particulate matter (PM) number concentrations, at the surrounding residential areas (Hudda and Fruin, 2016;
32 Hudda et al., 2016).

33 The dominant source of airport aerosol is aircraft engine exhaust (Kim, 2009), and is classified as either directly
34 emitted primary aerosol (PA) or secondary aerosol (SA). Due to the high combustion efficiency, PA from
35 aircraft engines contains mainly black carbon (BC) whereas SA is formed by the oxidation of emitted precursor
36 gases. PA and SA precursor emissions such as non-methane organic gases (NMOGs) strongly depend on aircraft
37 engine operating conditions (Kinsey et al., 2010) *e.g.* the BC emission index (EI, g/kg fuel) of a gas-turbine
38 engine is usually higher at cruise climb-out and take-off loads (above 60% of the maximum thrust) than at lower
39 loads used at idle, taxi (7%) and approach (30%) (Liati et al., 2014; Brem et al., 2015). In contrast to BC,
40 NMOG emissions, including *e.g.* aromatic hydrocarbons, aliphatic hydrocarbons and carbonyls, are clearly
41 highest at low loads (Spicer et al., 1994; Slemr et al., 2001; Anderson et al., 2006; Herndon et al., 2006; Kilic
42 et al., 2017).

43 Aging of fossil fuel combustion exhaust leads to SA/PA ratios higher than 1. Single-ring aromatics are
44 traditionally thought to be the most important secondary organic aerosol (SOA) precursors from combustion
45 emissions. While this has been shown to be the case for some emissions, *e.g.* from 2-stroke engines (Platt et al.,
46 2014), in other cases non-traditional precursors were assessed to be responsible for the bulk of the SOA mass
47 formed, *e.g.* for biomass smoke (Bruns et al., 2016) or on-road vehicles (Platt et al., 2013; 2017; Pieber et al.,
48 2017). Similar to these emissions, aging of aircraft emissions studied by Miracolo et al. (2011; 2012) in a smog
49 chamber produced substantial amounts of secondary PM exceeding primary PM emissions several-fold. The
50 authors showed the dominance of secondary organic aerosol (SOA) at low loads, while at high loads sulfate was
51 the main SA produced. While single-ring aromatic compounds determined using gas-chromatography/mass



52 spectrometry seemed to be important precursors of the SOA formed, a greater part of SOA was believed to
53 originate from non-traditional precursors, whose nature remains to be identified (Miracolo et al., 2011; 2012).
54 In this study, we measured the SA production potential of aircraft jet engine exhaust as a function of engine load
55 and examined the bulk gas-phase organic emissions and their SOA formation potential. SOA was produced by
56 OH-initiated oxidation of aircraft NMOG emissions in a potential aerosol mass (PAM) flow reactor (Kang et al.,
57 2007). Primary and secondary PM mass was characterized for different engine loads, using an aerosol mass
58 spectrometer (AMS). SOA precursors were analyzed in real-time by a proton-transfer-reaction mass
59 spectrometer (PTR-MS) and SOA closure was examined under different conditions. The impact of these
60 emissions and their SOA potential in typical urban atmospheres, at the proximity of airports is assessed and
61 compared to other mobile sources.

62 2 Methods

63 2.1 Experimental setup

64 Exhaust measurements were conducted to characterize NMOG and non-refractory submicron particulate mass
65 (NR-PM₁) emissions from an in-production CFM56 variant turbofan in the test cell of SR Technics at Zurich
66 Airport. The test engine was fueled with standard JET A-1 fuel, and was operated at several engine loads,
67 selected to represent aircraft activities during a typical landing/take-off (LTO) cycle. Engine loads were set by
68 specifying the combustion chamber inlet temperature values which correlate with a specific thrust (lbf) at
69 standard atmospheric conditions. The selected loads included idle-taxi (3-7% of the maximum thrust), approach
70 (30% of the maximum thrust), and an approximated cruise load (50-65% of the maximum static thrust). After
71 starting the engine, a warm-up sequence of 25 minutes ran before each test, consisting of five minute-long steps
72 at thrusts of 5%, 15%, 7%, 65% and 85% in sequence.

73 A simplified scheme of the experimental setup is shown in Figure 1 and is discussed in detail elsewhere (Kilic et
74 al., 2017). Details about the sampling system for non-volatile particle emissions can be found in Durdina et al.
75 (2017) and Brem et al. (2015). The turbine engine exhaust was sampled by a single-point probe with an inner
76 diameter of 8 mm, located 0.7 m downstream of the engine exit plane. The exhaust drawn by the probe was
77 directed through a heated (160°C) transfer line to three different lines: (i) the raw gas line, (ii) diluted emissions
78 line and (iii) diluted aged emissions line. CO, CO₂, and NO_x were measured by a multi-gas analyzer (PG250,
79 Horiba Inc.) installed on the raw line. On the diluted line, primary gas and particle measurements were
80 performed. Two ejector dilutors (DEKATI DI-1000) were installed in sequence on this transfer line; after the
81 first dilution, sampling lines were heated to 120°C. The sample was diluted with synthetic air (99.999% purity)
82 either by a factor of 10 or 100, depending on the NMOG concentration. The NMOGs were quantified and
83 characterized by a proton-transfer-reaction time-of-flight mass spectrometer (PTR-ToF-MS) together with a
84 flame ionization hydrocarbon detector (FID) (APHA 370 THC Monitor). The concentration of equivalent black
85 carbon (eBC) was determined by a 7-wavelength aethalometer (Drinovec et al., 2015) based on optical
86 absorption.

87 Aging of the engine exhaust emissions was achieved by using a potential aerosol mass (PAM) chamber with a
88 continuous flow of 7.6 l/min and a volume of 13.3 liters. Two mercury lamps (emission lines at wavelengths
89 $\lambda=182\text{ nm} - 254\text{ nm}$, BHK Inc.), mounted inside the PAM, were used to irradiate HONO and O₂ required for
90 hydroxyl radical (OH) formation. Different time-integrated OH exposures (molecules cm⁻³ h) were achieved by
91 modulating UV lamp intensity *e.g.* 80%, 90%, 100%. HONO to boost OH concentrations, and D9-butanol to
92 trace OH exposure (Barnet et al., 2012), were injected with flows of 1.8 and 0.4 l/min, respectively. Further, the
93 PAM was also humidified (~20% relative humidity) by injecting synthetic air with water vapor (with a flow of
94 1.6 l/min). All measurements were conducted at 295-298°K. Secondary aerosol formation was measured after
95 the PAM, while the primary emissions were measured from the bypass line.

96 Aging in a PAM is not completely analogous to that in a smog chamber, due to higher oxidant concentrations.
97 However, intercomparison studies suggest that the amount of SOA production and its bulk elemental
98 composition are comparable for both single precursors (*e.g.* α -pinene) (Lambe et al., 2015) and complex
99 emissions (*e.g.* wood combustion) (Bruns et al, 2015). In addition, in both the PAM and chambers, the dominant
100 oxidation pathways are similar to those in ambient air (Peng et al, 2015; 2016).

101 2.2 Instrumentation

102 2.2.1 PTR-ToF-MS

103 NMOGs having a higher proton affinity than water were quantified by a PTR-ToF-MS (PTR-TOF 8000,
104 Ionicon Analytik G.m.b.H., Innsbruck, Austria) (Jordan et al., 2009). NMOG molecules were positively charged
105 in the ionization unit (drift tube) of the instrument via hydronium ions (H₃O⁺), and the generated ions/fragments
106 were measured by a time-of-flight mass spectrometer. The PTR-ToF-MS utilized a drift voltage (Udrift) of 550
107 V, a drift chamber temperature (Tdrift) of 60°C and a drift pressure (pdrift) of 2.2 mbar, maintaining a reduced
108 electric field (E/N) of ~120 Townsends (Td). Data were collected with one second time resolution.



109 Tofware post-processing software (version 2.4.5, TOFWERK AG, Thun, Switzerland; PTR module as
110 distributed by Ionicon Analytik GmbH, Innsbruck, Austria), running in the Igor Pro 6.3 environment
111 (Wavemetrics Inc., Lake Oswego, OR, USA), was used for data analysis. The ion transmission function,
112 required to convert counts (cps) to volume mixing ratios (ppbv), was quantified using a gas standard containing
113 a mixture of 12 compounds (100 ppbv each) spanning mass-to-charge ratios (m/z) from m/z 33 to 181 (Carbagas
114 AG., Zurich, Switzerland). Volume mixing ratios (ppbv) were calculated according to De Gouw and Warneke,
115 2007, using H_3O^+ /NMOG reaction rate constants (k) from Cappellin et al., 2012, when available, and assuming
116 $2 \times 10^{-9} \text{ cm}^3 \text{ s}^{-1}$ otherwise.

117 During the exothermic proton-transfer reaction, some molecular fragments are formed in the drift chamber, with
118 the extent of fragmentation depending on the chamber conditions and functional groups in the molecules
119 (Gueneron et al., 2015). In particular, hydrocarbon fragments are obtained from aldehydes and dehydration of
120 some oxygenated ions. Assignment of these fragment ions to the corresponding parent ions is important for
121 quantification. The NMOG mixing ratios were corrected by accounting for this fragmentation. The compounds
122 were measured based on their parent ions, then their fragments were subtracted based on reference
123 fragmentation patterns. These subtractions combine a detailed fragmentation table for aldehydes using the
124 current drift chamber conditions from Klein et al. (2016) and fragmentation patterns for aromatic compounds
125 measured under similar chamber conditions reported ($E/N \sim 120 \text{ Td}$) in other studies (Buhr et al., 2002; Brown et
126 al., 2010; Gueneron et al., 2015). The fragmentation of detected compounds containing other functional groups
127 (e.g. hydrocarbons and non-aldehyde oxygenated compounds) cannot be fully excluded but are not expected to
128 cause significant error since the observed parent molecules were primarily low molecular weight alcohols and
129 acids (e.g. methanol, formic and acetic acid) that are less susceptible to fragmentation (de Gouw and Warneke,
130 2007). The NMOGs were then classified (acids, alcohols, aromatics, non-aromatics hydrocarbons and
131 unclassified hydrocarbon fragments, nitrogen and sulfur containing compounds, other oxygen containing
132 compounds, unidentified peaks) according to Kilic et al. (2017).

133 2.2.2 AMS

134 The condensed phase was continuously monitored before and after the PAM using a high resolution time-of-
135 flight aerosol mass spectrometer (AMS) and a scanning mobility particle sizer (SMPS). The reader is referred to
136 DeCarlo et al. (2006) for a more detailed description of the AMS operating principles, calibrations protocols,
137 and analysis procedures. Briefly, a particle beam sampled through an aerodynamic lens is alternately blocked
138 and unblocked, yielding the bulk particle mass spectra (MS mode) of the non-refractory (NR) species, including
139 organic aerosols (OA), NO_3^- , SO_4^{2-} , NH_4^+ , and Cl. The NR particles are flash vaporized by impaction on a
140 heated tungsten surface (heated to $\sim 600^\circ\text{C}$) at $\sim 10^{-7}$ Torr. The resulting gases are ionized by electron
141 ionization (EI, 70 eV) and the mass-to-charge ratios (m/z) of the fragments are determined by the ToF mass
142 spectrometer. The AMS was operated in the V-mode, with a time resolution of 30 sec. The AMS data were
143 analyzed using the SQUIRREL (version 1.52L) and PIKA (1.11L) analysis software in Igor Pro 6.3
144 (WaveMetrics). Standard relative ionization efficiencies (RIE) were assumed for the organic aerosol and
145 chloride (RIE = 1.4, and 1.3, respectively) and experimentally determined for sulfate and ammonium (RIE =
146 ~ 1.1 and ~ 4 , respectively). The collection efficiency due to the particle bounce was determined to be ~ 1 under
147 our conditions for organic rich aerosols by comparing the AMS mass to the SMPS volume (assuming an OA
148 density of 1.4).

149 2.3 Data analysis

150 Emissions from the aircraft turbofan were measured at different thrust levels referred to as “test points”
151 hereinafter. Test point durations were 18 minutes, except for one 60 minute-long run. Test points were
152 systematically interspersed with five minute-long periods to clean the PAM and the transfer lines by flushing the
153 setup with synthetic air. The averaging of the primary emissions started from the third minute of a test point
154 when the engine operation was stable. After sampling primary emissions for five to eight minutes while
155 bypassing the PAM, secondary formation was measured after the PAM during the last five to eight minutes of
156 the test point. This allows SOA to reach a steady state in the PAM. During each test, the PA concentration was
157 measured by bypassing the PAM, while the SA concentration was calculated by subtracting PA from the OA
158 measured after aging (after the PAM). Both PA and SA concentrations were determined by AMS.
159 The expected SOA concentration from the sum of all NMOGs detected by the PTR-ToF-MS was also calculated
160 by multiplying the NMOGs oxidized in the PAM by its corresponding SOA yields, according to Eq. 1:



$$161 \quad \sum_{i=1}^n SOA_{modelled} = \sum_{i=1}^n \Delta NMOG_i \times Yield_i \quad \text{Eq. 1,}$$

162 where n is the number of NMOGs quantified and $\Delta NMOG$ is the difference between the primary NMOG
 163 concentration and the NMOG concentration after aging. The same approach was applied by Bruns et al. (2016)
 164 and yields used can be found in Table 2. SOA yields available in the literature were used when possible.
 165 Otherwise, SOA yields of 0.2 were assumed as a lower limit estimate for aromatic and oxy-aromatics for which
 166 no SOA-yield values were reported (Presto et al., 2010; Tkacik et al., 2012), similar to Bruns et al. (2016). A
 167 yield of 0.15 was assumed for other NMOGs, including non-aromatic hydrocarbons and carbonyls. As NO is
 168 completely consumed in the PAM, we have chosen yields from low NO_x conditions for aromatic hydrocarbons
 169 (Ng et al., 2007; Chan et al., 2009; Hildebrandt et al., 2009; Nakao et al., 2011). The SOA contribution from
 170 organic gases lighter than benzene (C₆H₆) was neglected. Predicted NMOG contributions to SOA are provided
 171 in the Results section.

172 Emission indices (EI , g/kg fuel) were calculated using a mass balance on fuel carbon:

$$173 \quad EI = [X] \times \left[\frac{MW_{CO_2}}{MW_C \times \Delta CO_2} + \frac{MW_{CO}}{MW_C \times \Delta CO} \right] \times C_f \quad \text{Eq. 1,}$$

174 where X denotes the pollutant concentration ($\mu\text{g}/\text{m}^3$) and MW (g/mole) is the molecular weight of the species
 175 denoted by the subscript. Background-subtracted CO and CO₂ concentrations ($\mu\text{g}/\text{m}^3$) are denoted as ΔCO and
 176 ΔCO_2 , respectively. C_f is the carbon fraction of the JET-A1 fuel used during the campaign and was measured as
 177 0.857 based on ASTM D 5291 method (ASTM, 1996).

178 3 Results and discussion

179 3.1 SOA formation as a function of OH exposure

180 The evolution of the chemical composition of the primary organic gases and NR-PM₁ components with
 181 increasing OH exposure is shown in Figure 2 for engine idling operation (thrust 3%). Measurements were
 182 conducted for primary emissions, as well as for OH exposures of 59×10^6 , 88×10^6 , and 113×10^6 molecules cm⁻³
 183 h, which correspond to approximately 39, 58, and 75 hours of atmospheric aging under an average tropospheric
 184 OH concentration of 1.5×10^6 molecules cm⁻³ (Mao et al., 2009). The OH exposure, calculated using d9-
 185 butanol as a tracer, was varied by varying the light intensity.

186 Figure 2a shows the OG composition under these conditions with compounds classified as a function of their
 187 molecular composition, as described in Kilic et al. (2017). A stepwise increase of the OH exposure reduced the
 188 NMOG mass detected in the chamber by 35%, 40% and 50%. Except for carboxylic acids, the concentrations of
 189 all NMOGs decreased during aging, indicating that their loss rate exceed their production from other NMOGs.
 190 For example, aromatic compounds and carbonyls were oxidized in the PAM by up to 90% and 50%,
 191 respectively, while the acids doubled after 75 hours of daytime-equivalent aging.

192 Figure 2b shows a time series of secondary NR-PM₁ composition, as well as the concentrations of two of the most
 193 abundant aromatic gases, C₁₀H₁₄ and C₁₁H₁₆, for the same experiment. Here stable oxidation conditions
 194 were alternated with sampling of primary emissions, with OH exposures indicated in the figure. Secondary
 195 aerosol, especially SOA, dominated the total NRPM₁. By increasing the OH exposure from 59×10^6 to 88×10^6 ,
 196 the generated SOA increased by approximately 14%. However, increasing the OH exposure further to 113×10^6
 197 molecules cm⁻³ h yielded only an additional 3% increase in SOA mass. This suggests that at these OH
 198 exposures, the bulk of SOA precursors have reacted and the additional SOA production did not significantly
 199 exceed its loss. Under these conditions, the formed SOA may be considered as a reasonable estimate for the
 200 total SOA potential. The observed production rate of SOA against OH exposure is consistent with precursor
 201 reaction rates of 8×10^{-12} molecule⁻¹ cm³ s⁻¹. This estimate is based on the assumption of a constant SOA mass
 202 yield with aging and instantaneous equilibrium partitioning of the condensable gases, and is therefore lower than
 203 the reaction rates of the main identified precursors (see below). SOA production rates are thus expected to be
 204 faster in the ambient atmosphere.

205 3.2 Particle and gaseous emissions as a function of engine load

206 Figure 3 shows both average primary and secondary emissions indices for varying engine loads (left) and EIs
 207 from individual test points (right). The NMOG EI decreased from 30 to 0.8 g/kg fuel when the thrust level
 208 increased from 3-5% to 90%. At thrust 3-5%, the emissions of gaseous aromatic-hydrocarbons were highest
 209 (with an EI of ~5g/kg fuel) and decreased with increasing thrust (with an EI of ~0.15 g/kg fuel at thrust 90%).
 210 Similar to aromatic gases, SOA were formed mostly at 3-5% thrust and had a declining trend with thrust.
 211 In contrast, BC, POA and secondary SO₄ EIs were highest during the approximated cruise load (thrust 60%). At



212 these conditions, secondary NR-PM₁ was mostly inorganic and SOA mass was comparable to that of primary
213 carbonaceous emissions (BC + POA). SOA was approximately 100 times higher than POA at idle and only 10
214 times higher at cruise (Figure 3). This dependence of the aged aerosol composition on the thrust level, obtained
215 using the PAM reactor, confirm quite readily the previous results obtained in a smog chamber (Miracolo et al.,
216 2011; 2012).

217 3.3 Precursor gases of SOA: Idling

218 Single-ring aromatics, such as xylenes, methylbenzenes, toluene, and benzene, were previously linked with
219 SOA formation (e.g. (Odum et al., 1997; Ng et al., 2007)). These aromatic gases are important contributors in the
220 emissions from combustion sources such as two-stroke scooters (Platt et al., 2013), or wood burning (Bruns et
221 al., 2016). Idling exhaust contained 20% (mass weighted) of aromatic HCs. Figure 4 presents the mass fractions
222 of aromatic hydrocarbons in primary exhaust for an idling turbine engine. More than half of the aromatic
223 hydrocarbons emitted were single-ring aromatics. 75 - 95% of these aromatics were oxidized with an OH
224 exposure of $\sim 90 \times 10^6$ molecules cm^{-3} h in the PAM.

225 By using previously reported SOA yields (Table 2) for NMOGs, SOA production was predicted from individual
226 precursors according to Eq. 1. Figure 5 shows a comparison of the predicted SOA with the SOA determined by
227 AMS measurements (top) and the predicted SOA contribution by the oxidation of NMOGs in the PAM
228 (bottom), for two idling thrusts, 2-5% (left) and 6-7% (right). The predicted SOA from the NMOGs reacted are
229 shown at the bottom panel of the figure and compound class-specific SOA fractions are separated for aromatic
230 HCs, oxygenated-aromatics, other HCs, N-containing OGs and other OGs.

231 Results in Figure 5 indicate that the most important SOA precursors emitted by turbine engines at idle are
232 aromatic hydrocarbons such as benzene derivatives but also oxygenated aromatics such as phenol. The predicted
233 SOA formed by aromatics alone, both by aromatic hydrocarbons (60-70%) and oxygenated-aromatics (15-25%),
234 explained all AMS-determined SOA at low loads (thrust 3-5%) and most of the SOA formed (by 80%) at idle 6-
235 7% (Figure 5). Predicted aromatic SOA from benzene (C₆H₆), C2-benzenes (C₈H₁₀), C3-benzenes (C₉H₁₂), C4-
236 benzenes (C₁₀H₁₄), dimethylstyrenes (C₁₀H₁₂), toluene (C₇H₈), methylbenzaldehydes (C₈H₈O) and phenol
237 (C₆H₆O) accounted for 60% of the AMS-determined SOA at 3-5% thrust (Figure 5). These results are consistent
238 with those previously obtained using a smog chamber, confirming that aromatic compounds are indeed
239 important SOA precursors in jet-engine emissions (Miracolo et al., 2011). Only a small fraction of these
240 compounds was determined in previous experiments using GC/MS measurements and therefore traditionally
241 considered as SOA precursors in models. Here, compared to previous experiments we show that non-traditional
242 aromatic and oxy-aromatic compounds, including naphthalene and its alkyl derivatives, C>3 alkyl derivatives of
243 single ring aromatics, and phenols, can explain the gap between measured SOA and SOA predicted based on
244 traditional precursors.

245 Exhaust-aging experiments were repeated 6 times at thrust 3-5% and the oxidation of NMOGs varied during
246 each of these aging experiments. Error bars shown in Figure 5 denote this variability in NMOG oxidation (in the
247 PAM) during aging experiments of the same thrust level. Indeed, errors related to yield values used may
248 significantly influence the results. These errors may be systematic and are complex to assess. They can be
249 affected by potential differences between the oxidation conditions in chambers and in the PAM (e.g. NOx, RH,
250 particle mass). Yields obtained with the PAM are consistent with those obtained from chambers (Bruns et al.,
251 2015), therefore we do not expect large systematic errors in the SOA predicted. However, based on the
252 variability of yields in previous chamber experiments we estimate the accuracy of our prediction to be within a
253 factor of 2, indicating that within our uncertainties a significant fraction of the precursors was identified.
254 NMOGs, including aromatic gases, were reduced with increasing thrust (from thrust 3-5% to thrust 6-7%) due
255 to more efficient operation of the turbine engine. This decrease amounted to 40% for the sum of aromatic HCs
256 and corresponded to a 30% decrease in SOA EI. Therefore, a more efficient engine operation implies less
257 NMOG emissions and reduced SOA formation potential at idle.

258 3.4 SOA formation at an approximated cruise load

259 A comparison of the predicted SOA with the SOA determined by the AMS is presented in Figure 6 at cruise
260 loads (top panel). Figure 6 also shows the SOA contribution predicted by the oxidation of NMOGs in the PAM
261 (bottom panel) under the same engine conditions. The SOA EI was 0.07 g/kg fuel for cruise load. The predicted
262 SOA fraction accounted for only 30% of the AMS-determined SOA (green bar, Figure 6) during cruise load
263 experiments. Aromatic SOA (predicted) accounted for only 4% of the AMS-determined SOA during these
264 experiments. The major fraction of the remaining SOA mass that was assigned to the identified precursors was
265 predicted to be from oxygenated NMOG molecules (Figure 6). Another 6% of the determined SOA may
266 originate from non-aromatic HCs (aliphatics and HC fragments > C₆).

267 Predicted SOA was significantly lower compared to the measured SOA. While SOA precursors remain
268 unidentified under these conditions, several hypotheses might explain the observation. First, we could not
269 determine the contribution of alkanes smaller than 9 carbon atoms to the formed SOA, because these



270 compounds are not directly detected by the PTR-ToF-MS. Depending on the number of carbon atoms in their
271 molecular structure, the SOA potential of many alkanes may be comparable to that of single-ring aromatic
272 hydrocarbons (Tkacik et al., 2012) and therefore may play a role in the formation of the observed SOA.
273 However, our data do not suggest that a great part of the observed SOA is from non-measured alkanes, as we do
274 not observe any increase in the contribution of hydrocarbon fragments in the PTR-MS compared to idling
275 emissions. Second, the oxidation of primary semi-volatile compounds may yield significant SOA, because of
276 their elevated yields of near unity (Robinson et al., 2007). However, we note that these semi-volatile precursors
277 would play an important role at low aerosol concentrations, when most of these precursors reside in the gas-
278 phase where they can be oxidized. Under our conditions, concentrations range between 10 and 50 $\mu\text{g m}^{-3}$ and a
279 substantial fraction of these products resides already in the particle phase. Therefore the oxidation of these
280 products in the gas-phase by OH is unlikely to explain the observed entire 10-fold increase in the OA mass upon
281 oxidation, but only part of the mass. Finally, the PTR-MS data suggest that a great part of the precursors
282 measured are highly oxygenated gases, with O:C ratios ranging from 0.2 to 0.7, including, among others,
283 anhydrides (*e.g.* phthalic, succinic and maleic) and quinone derivatives. Unlike aromatic compounds and
284 alkanes present in the fuel, these compounds are likely formed at high temperature during combustion. The SOA
285 yields of these compounds remain unknown and it is likely that the yield value of 0.15 used here is a lower
286 estimate, which would result in an underestimation of the contribution of these compounds to the observed
287 SOA. We also note that unlike precursors detected under idle conditions, the ionization efficiency and the
288 fragmentation pattern of these compounds in the PTR-MS are highly uncertain, resulting in large uncertainties
289 in our predicted SOA. Therefore, results in Figure 6 should be considered with care. Notwithstanding these
290 uncertainties, we note that at cruise conditions the SOA contribution to the total secondary PM is minor
291 compared to sulfate and therefore these uncertainties have little impact on the implications of our results.

292 4 Conclusions and implications for ambient air quality

293 Gas-phase primary emissions and SA formation from an in-production turbofan were investigated in a test cell.
294 The engine loads (thrusts) during experiments were selected to simulate different aircraft operations. These
295 operations are summarized as landing take-off (LTO) cycle under four modes taxi/idle, approach, climb and
296 take-off with corresponding engine loads of 3-7%, 30%, 85% and 100%, respectively. In addition an
297 approximated cruising load (60%) was selected.

298 At idle conditions, SOA formation was mostly attributed to the oxidative processing of aromatic gases. Benzene
299 derivatives together with phenol were predicted as the major SOA precursors for an idling aircraft. Meanwhile,
300 during cruise load the emission of aromatic compounds was much lower and only explained a minor fraction of
301 SOA (4%). During these conditions, however, sulfate was found to dominate SA, contributing ~85% of the total
302 mass of aged aerosols and therefore its fraction is more relevant aloft.

303 The oxidation of NMOGs in the PAM yielded a SOA EI 100 times greater than POA under idling conditions
304 and 10 times greater at cruise load. According to our calculated production rates SOA from airport emissions
305 (idling jet engines) exceeds POA by a factor of 10 after only 3 hours of atmospheric aging and therefore
306 considerably impacts urban areas downwind of airport emissions. Compared to idling aircraft emissions, aging
307 of vehicle exhaust emissions results in much lower enhancements, ranging between factors of 5-10 and 1.5-3,
308 for gasoline and diesel vehicles, respectively (Gordon et al., 2014a; 2014b).

309 The NMOG emission factors and SOA potential can be used in conjunction with emission inventories and fuel
310 use data to assess the impact of aircraft emissions on air quality in comparison with other mobile sources. Here,
311 we have considered the Zurich international airport as an example (Switzerland, 23 million passengers in 2010).
312 Combining the recorded aircraft fuel use with the standard LTO cycle and the NMOG EIs measured, we
313 estimate aircraft NMOG emissions in Zurich for 2010 to be in the range of 90–190 tons/year (Kilic et al., 2017).
314 Based on the average SOA bulk yields (SOA/total NMOG) obtained herein (~5-8%), we estimate a total SOA
315 production potential from airport emissions for the area of Zurich to range from 5.4 to 13.2 tons/year. These
316 SOA production potential values can be directly compared to emissions from on-road vehicles derived from the
317 EDGARv4.2 emission inventory, which provides worldwide temporally and spatially resolved NMOG
318 emissions from road vehicles with a grid size of ~200 km^2 . For the grid cell containing Zurich (47.25° North,
319 8.75° East) the NMOG emissions from on-road vehicles is estimated to be 631 tons/year. While SOA yields
320 from diesel vehicle emissions are expected to be more elevated than those from gasoline car emissions, due to
321 the presence of intermediate volatility species, recent reports suggest these yields to be comparably high, ~15%
322 (Gentner et al., 2017). Using this yield value for emissions from both types of vehicles (Platt et al., 2017), we
323 estimate the total SOA production potential from on road vehicles for the area of Zurich to be ~94 tons/year, 10
324 fold higher than SOA from aircraft emissions. However, the airport is a point source within this region and thus
325 the relative contribution of the airport emissions to a specific location downwind of this source is significantly
326 higher than implied by this calculation. Although this estimate applies to a specific airport, it does indicate that
327 aircraft NMOG emissions may constitute significant SOA precursors downwind of airports, while other fossil
328 fuel combustion sources dominate urban areas in general.

329 **Acknowledgements**

330 Funding was provided by the Swiss Federal Office of Civil Aviation (FOCA). This project would not have been
331 possible without the support of Rene Richter (PSI) and SR Technics personnel. Many individuals from SR
332 Technics contributed to the project but we owe special thanks to those from the Maintenance and Test Cell
333 Group. JGS acknowledges support from the Swiss National Science Foundation starting grant BSSG10_155846.
334

335 **References**

- 336 (Alvarez et al., 2009) Alvarez, E. G., Borrás, E., Viidanoja, J., & Hjorth, J. (2009). Unsaturated dicarbonyl
337 products from the OH-initiated photo-oxidation of furan, 2-methylfuran and 3-methylfuran. *Atmos. Environ.*,
338 43(9), 1603–1612.
- 339 (Anderson et al., 2006) Anderson, B. E., Chen, G., & Blake, D. R. (2006). Hydrocarbon emissions from a
340 modern commercial airliner. *Atmos. Environ.*, 40(19), 3601–3612.
- 341 (ASTM, 1996) ASTM, D. (1996). 5291 (1996) standard test methods for instrumental determination
342 of carbon, hydrogen, and nitrogen in petroleum products and lubricants. *ASTM, West Conshohocken*.
- 343 (Barmet et al., 2012) Barmet, P., Dommen, J., DeCarlo, P., Tritscher, T., Praplan, A., Platt, S., Prévôt, A.,
344 Donahue, N., & Baltensperger, U. (2012). OH clock determination by proton transfer reaction mass
345 spectrometry at an environmental chamber. *Atmos. Meas. Tech.*, 5(3), 647–656.
- 346 (Brem et al., 2015) Brem, B. T., Durdina, L., Siegerist, F., Beyerle, P., Bruderer, K., Rindlisbacher, T.,
347 Rocci-Denis, S., Andac, M. G., Zelina, J., Penanhoat, O., & Wang, J. (2015). Effects of fuel aromatic content on
348 nonvolatile particulate emissions of an in-production aircraft gas turbine. *Environ. Sci. Technol.*, 49(22), 13149–
349 13157.
- 350 (Brown et al., 2010) Brown, P., Watts, P., Märk, T., & Mayhew, C. (2010). Proton transfer reaction mass
351 spectrometry investigations on the effects of reduced electric field and reagent ion internal energy on product
352 ion branching ratios for a series of saturated alcohols. *Int. J. Mass Spectrom.*, 294(2), 103–111.
- 353 (Bruns et al., 2015) Bruns, E., El Haddad, I., Keller, A., Klein, F., Kumar, N., Pieber, S., Corbin, J.,
354 Slowik, J., Brune, W., Baltensperger, U. & Prévôt, A. S. H. (2015). Inter-comparison of laboratory smog
355 chamber and flow reactor systems on organic aerosol yield and composition. *Atmos. Meas. Tech.*, 8(6), 2315–
356 2332.
- 357 (Bruns et al., 2016) Bruns, E. A., El Haddad, I., Slowik, J. G., Kilic, D., Klein, F., Baltensperger, U., &
358 Prévôt, A. S. H. (2016). Identification of significant precursor gases of secondary organic aerosols from
359 residential wood combustion. *Sci. Rep.*, 6, 27881, doi:10.1038/srep27881.
- 360 (Buhr et al., 2002) Buhr, K., van Ruth, S., & Delahunty, C. (2002). Analysis of volatile flavour
361 compounds by proton transfer reaction-mass spectrometry: fragmentation patterns and discrimination between
362 isobaric and isomeric compounds. *Int. J. Mass Spectrom.*, 221(1), 1–7.
- 363 (Chan et al., 2010) Chan, A., Chan, M., Surratt, J. D., Chhabra, P., Loza, C., Crouse, J., Yee, L., Flagan,
364 R., Wennberg, P., & Seinfeld, J. (2010). Role of aldehyde chemistry and NO_x concentrations in secondary
365 organic aerosol formation. *Atmos. Chem. Phys.*, 10(15), 7169–7188.
- 366 (Chan et al., 2009) Chan, A. W. H., Kautzman, K. E., Chhabra, P. S., Surratt, J. D., Chan, M. N.,
367 Crouse, J. D., Kürten, A., Wennberg, P. O., Flagan, R. C., & Seinfeld, J. H. (2009). Secondary organic aerosol
368 formation from photooxidation of naphthalene and alkylnaphthalenes: implications for oxidation of intermediate
369 volatility organic compounds (IVOCs). *Atmos. Chem. Phys.*, 9(9), 3049–3060.
- 370 (Chhabra et al., 2011) Chhabra, P., Ng, N., Canagaratna, M., Corrigan, A., Russell, L., Worsnop, D., Flagan,
371 R., & Seinfeld, J. (2011). Elemental composition and oxidation of chamber organic aerosol. *Atmos. Chem.*
372 *Phys.*, 11(17), 8827–8845.
- 373 (de Gouw & Warneke, 2007) de Gouw, J. & Warneke, C. (2007). Measurements of volatile organic
374 compounds in the Earth's atmosphere using proton-transfer-reaction mass spectrometry. *Mass Spectrom. Rev.*,
375 26(2), 223–257.
- 376 (Drinovec et al., 2015) Drinovec, L., Mocnik G., Zotter P., Prevot A. S. H., Ruckstuhl C., Coz E., Rupakheti
377 M., Sciare J., Muller T., Wiedensohler A., and Hansen A. D. A. (2015) The "dual-spot" Aethalometer: an
378 improved measurement of aerosol black carbon with real-time loading compensation, *Atmos. Meas. Tech.*, 8(5),
379 1965-1979.



- 380 (Gentner et al., 2017) Gentner D. R., Shantanu H. Jathar H. S., Gordon D. T., Bahreini R., Day D. A., Imad
381 El Haddad, Hayes P. L., Pieber S. M., Platt S. M., de Gouw J., Goldstein H. A., Harley R. A., Jimenez L. J.,
382 Prévôt A. S. H., and Robinson L. A. (2017). Review of urban secondary organic aerosol formation from
383 gasoline and diesel motor vehicle emissions, *Environ. Sci. Technol.*, 51 (3), 1074–1093. doi:
384 10.1021/acs.est.6b04509
- 385 (Gordon et al., 2014a) Gordon, T., Presto, A., Nguyen, N., Robertson, W., Na, K., Sahay, K., Zhang, M.,
386 Maddox, C., Rieger, P., Chattopadhyay, S., Maldonado, H., Maricq, M. M., and Robinson, A. L. (2014a).
387 Secondary organic aerosol production from diesel vehicle exhaust: impact of aftertreatment, fuel chemistry and
388 driving cycle. *Atmos. Chem. Phys.*, 14(9), 4643–4659.
- 389 (Gordon et al., 2014b) Gordon, T. D., Presto, A. A., May, A. A., Nguyen, N. T., Lipsky, E. M., Donahue,
390 N. M., Gutierrez, A., Zhang, M., Maddox, C., Rieger, P., Chattopadhyay, S., Maldonado, H., Maricq, M. M., &
391 Robinson, A. L. (2014b). Secondary organic aerosol formation exceeds primary particulate matter emissions for
392 light-duty gasoline vehicles. *Atmos. Chem. Phys.*, 14(9), 4661–4678.
- 393 (Gueneron et al., 2015) Gueneron, M., Erickson, M. H., VanderSchelden, G. S., & Jobson, B. T. (2015).
394 PTR-MS fragmentation patterns of gasoline hydrocarbons. *Int. J. Mass Spectrom.*, 379, 97–109.
- 395 (Herndon et al., 2006) Herndon, S. C., Rogers, T., Dunlea, E. J., Jayne, J. T., Miake-Lye, R., & Knighton, B.
396 (2006). Hydrocarbon emissions from in-use commercial aircraft during airport operations. *Environ. Sci.*
397 *Technol.*, 40(14), 4406–4413.
- 398 (Hildebrandt et al., 2009) Hildebrandt, L., Donahue, N. M., & Pandis, S. N. (2009). High formation of
399 secondary organic aerosol from the photo-oxidation of toluene. *Atmos. Chem. Phys.*, 9(9), 2973–2986.
- 400 (Hudda & Fruin, 2016) Hudda, N. & Fruin, S. (2016). International airport impacts to air quality: Size and
401 related properties of large increases in ultrafine particle number concentrations. *Environ. Sci. Technol.*, 50(7),
402 3362–3370.
- 403 (Hudda et al., 2014) Hudda, N., Gould, T., Hartin, K., Larson, T. V., & Fruin, S. A. (2014). Emissions
404 from an international airport increase particle number concentrations 4-fold at 10 km downwind. *Environ. Sci.*
405 *Technol.*, 48(12), 6628–6635.
- 406 (Hudda et al., 2016) Hudda, N., Simon, M., Zamore, W., Brugge, D., & Durant, J. (2016). Aviation
407 emissions impact ambient ultrafine particle concentrations in the Greater Boston area. *Environ. Sci. Technol.*,
408 2016, 50 (16), 8514–8521.
- 409 (Jordan et al., 2009) Jordan, A., Haidacher, S., Hanel, G., Hartungen, E., Märk, L., Seehauser, H.,
410 Schottkowsky, R., Sulzer, P., & Märk, T. (2009). A high resolution and high sensitivity proton-transfer-reaction
411 time-of-flight mass spectrometer (PTR-ToF-MS). *Int. J. Mass Spectrom.*, 286(2), 122–128.
- 412 (Kang et al., 2007) Kang, E., Root, M., Toohey, D., & Brune, W. (2007). Introducing the concept of
413 potential aerosol mass (PAM). *Atmos. Chem. Phys.*, 7(22), 5727–5744.
- 414 (Kilic et al., 2017) Kilic, D., Brem, B. T., Klein, F., El-Haddad, I., Durdina, L., Rindlisbacher, T.,
415 Setyan, A., Huang, R., Wang, J., Slowik, J. G., Baltensperger, U., & Prevot, A. S. H. (2017). Characterization of
416 gas-phase organics using proton transfer reaction time-of-flight mass spectrometry: Aircraft turbine engines.
417 *Environ. Sci. Technol.*, 2017, 51 (7), 3621–3629. doi: 10.1021/acs.est.6b04077
- 418 (Kim, 2009) Kim, B. Y. (2009). Guidebook on Preparing Airport Greenhouse Gas Emissions
419 Inventories, volume 11. *Transportation Research Board*.
- 420 (Kinsey et al., 2010) Kinsey, J. S., Dong, Y., Williams, D. C., & Logan, R. (2010). Physical
421 characterization of the fine particle emissions from commercial aircraft engines during the aircraft particle
422 emissions experiment (APEX) 1–3. *Atmos. Environ.*, 44(17), 2147–2156.
- 423 (Kuenen et al., 2014) Kuenen, J. J. P., Visschedijk, A. J. H., Jozwicka, M., & Denier van der Gon, H. A. C.
424 (2014). TNO-MACC_II emission inventory; a multi-year (2003–2009) consistent high-resolution European
425 emission inventory for air quality modelling. *Atmos. Chem. Phys.*, 14(20), 10963–10976.
- 426 (Lambe et al., 2015) Lambe, A., Chhabra, P., Onasch, T., Brune, W., Hunter, J., Kroll, J., Cummings, M.,
427 Brogan, J., Parmar, Y., Worsnop, D., et al. (2015). Effect of oxidant concentration, exposure time, and seed
428 particles on secondary organic aerosol chemical composition and yield. *Atmos. Chem. Phys.*, 15(6), 3063–3075.
- 429 (Liati et al., 2014) Liati, A., Brem, B. T., Durdina, L., Vögtli, M., Dasilva, Y. A. R., Eggenchwiler,
430 P. D., & Wang, J. (2014). Electron microscopic study of soot particulate matter emissions from aircraft turbine
431 engines. *Environ. Sci. Technol.*, 48(18), 10975–10983.



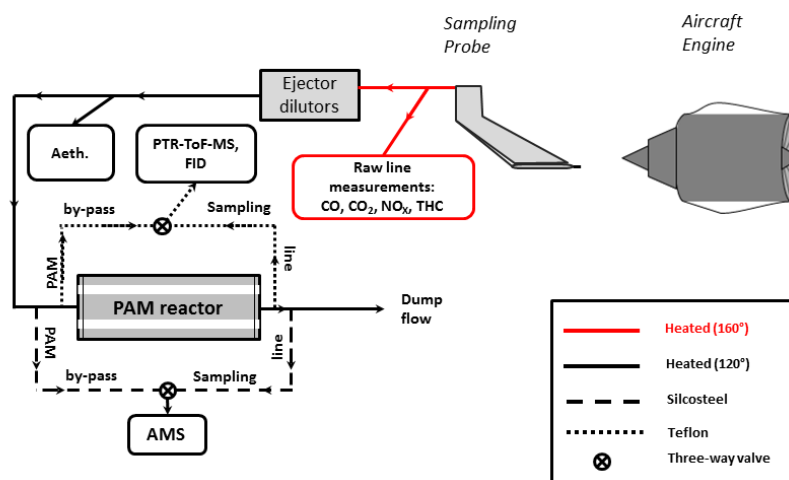
- 432 (Lin et al., 2008) Lin, S., Munsie, J., Herdt-Losavio, M., Hwang, S., Civerolo, K., McGarry, K., &
433 Gentile, T. (2008). Residential proximity to large airports and potential health impacts in New York State. *Int.*
434 *Arch. Occup. Environ. Health.*, 81(7), 797–804.
- 435 (Mao et al., 2009) Mao, J., Ren, X., Brune, W., Olson, J., Crawford, J., Fried, A., Huey, L., Cohen, R.,
436 Heikes, B., Singh, H., et al. (2009). Airborne measurement of OH reactivity during INTEX-B. *Atmos. Chem.*
437 *Phys.*, 9(1), 163–173.
- 438 (Miracolo et al., 2011) Miracolo, M., Hennigan, C., Ranjan, M., Nguyen, N., Gordon, T., Lipsky, E., Presto,
439 A., Donahue, N., & Robinson, A. (2011). Secondary aerosol formation from photochemical aging of aircraft
440 exhaust in a smog chamber. *Atmos. Chem. Phys.*, 11(9), 4135–4147.
- 441 (Miracolo et al., 2012) Miracolo, M. A., Drozd, G. T., Jathar, S. H., Presto, A. A., Lipsky, E. M., Corporan,
442 E., & Robinson, A. L. (2012). Fuel composition and secondary organic aerosol formation: Gas-turbine exhaust
443 and alternative aviation fuels. *Environ. Sci. Technol.*, 46(15), 8493–8501.
- 444 (Nakao et al., 2011) Nakao, S., Clark, C., Tang, P., Sato, K., & Cocker III, D. (2011). Secondary organic
445 aerosol formation from phenolic compounds in the absence of NO_x. *Atmos. Chem. Phys.*, 11(20), 10649–10660.
- 446 (Ng et al., 2007) Ng, N., Kroll, J., Chan, A., Chhabra, P., Flagan, R., & Seinfeld, J. (2007). Secondary
447 organic aerosol formation from m-xylene, toluene, and benzene. *Atmos. Chem. Phys.*, 7(14), 3909–3922.
- 448 (Odum et al., 1997) Odum, J. R., Jungkamp, T. P. W., Griffin, R. J., Forstner, H. J. L., Flagan, R. C., &
449 Seinfeld, J. H. (1997). Aromatics, reformulated gasoline, and atmospheric organic aerosol formation. *Environ.*
450 *Sci. Technol.*, 31(7), 1890–1897.
- 451 (Peng et al., 2016) Peng, Z., Day, D. A., Ortega, A. M., Palm, B. B., Hu, W., Stark, H., Li, R., Tsigaridis,
452 K., Brune, W. H., & Jimenez, J. L. (2016). Non-OH chemistry in oxidation flow reactors for the study of
453 atmospheric chemistry systematically examined by modeling. *Atmos. Chem. Phys.*, 16(7), 4283–4305.
- 454 (Peng et al., 2015) Peng, Z., Day, D. A., Stark, H., Li, R., Lee-Taylor, J., Palm, B. B., Brune, W. H., &
455 Jimenez, J. L. (2015). HO_x radical chemistry in oxidation flow reactors with low-pressure mercury lamps
456 systematically examined by modeling. *Atmos. Meas. Tech.*, 8(11), 4863–4890.
- 457 (Pieber et al., 2017) Simone M. Pieber, Nivedita K. Kumar, Felix Klein, Pierre Comte, Deepika Bhattu,
458 Josef Dommen, Emily A. Brun, Dogushan Kilic, Alejandro Keller, Urs Baltensperger, Jan Czerwinski, Norbert
459 Heeb, Jay G. Slowik and André S. H. Prévôt. Gas phase composition and secondary organic aerosol formation
460 from gasoline direct injection vehicles investigated in a batch and flow reactor: effects of prototype gasoline
461 particle filters. *Atmos. Chem. Phys. Discuss.*, in review, 2017.
- 462 (Platt et al., 2013) Platt, S. M., El Haddad, I., Zardini, A. A., Clairotte, M., Astorga, C., Wolf, R.,
463 Slowik, J. G., Temime-Roussel, B., Marchand, N., Ježek, I., Drinovec, L., Močnik, G., Möhler, O., Richter, R.,
464 Barmet, P., Bianchi, F., Baltensperger, U., & Prévôt, A. S. H. (2013). Secondary organic aerosol formation from
465 gasoline vehicle emissions in a new mobile environmental reaction chamber. *Atmos. Chem. Phys.*, 13(18),
466 9141–9158.
- 467 (Platt et al., 2014) Platt, S. M., El Haddad, I., Pieber, S. M., Huang, R.-J., Zardini, A., Clairotte, M.,
468 Suarez-Bertoa, R., Barmet, P., Pfaffenberger, L., Wolf, R., Slowik, J. G., Fuller, S. J., Kalberer, M., Chirico, R.,
469 Dommen, J., Astorga, C., Zimmermann, N., Marchand, N., Hellebust, S., Temime-Roussel, B., Baltensperger,
470 U. & Prévôt, A. S. H. (2014). Two-stroke scooters are a dominant source of air pollution in many cities, *Nat.*
471 *Commun.*, 5, 3749.
- 472 (Platt et al., 2017) Platt, S. M., El Haddad, I., Pieber, S. M., Zardini, A., Clairotte, M., Suarez-Bertoa
473 R., Daellenbach, K.R., Huang, R.-J., Slowik, J. G., Hellebust S., Temime-Roussel B., Marchand N., de Gouw J.,
474 Jimenez J.L., Hayes P. L., Robinson A. L., Baltensperger U., Astorga C. Prévôt, A. S. H. (2017). Gasoline cars
475 produce more carbonaceous particulate matter than modern filter-equipped diesel cars, *Sci. Rep.*, 7, 4926.
- 476 (Presto et al., 2010) Presto, A. A., Miracolo, M. A., Donahue, N. M., & Robinson, A. L. (2010).
477 Secondary organic aerosol formation from high-NO_x photo-oxidation of low volatility precursors: n-alkanes.
478 *Environ. Sci. Technol.*, 44(6), 2029–2034.
- 479 (Robinson et al., 2007) Robinson, A. L., Donahue, N. M., Shrivastava, M. K., Weitkamp, E. A., Sage, A. M.,
480 Grieshop, A. P., Lane, T. E., Pierce, J. R., & Pandis, S. N. (2007). Rethinking organic aerosols: Semivolatile
481 emissions and photochemical aging. *Science*, 315(5816), 1259–1262.
- 482 (Shakya & Griffin, 2010) Shakya, K. M. & Griffin, R. J. (2010). Secondary organic aerosol from
483 photooxidation of polycyclic aromatic hydrocarbons. *Environ. Sci. Technol.*, 44(21), 8134–8139.



- 484 (Slemr et al., 2001) Slemr, F., Giehl, H., Habram, M., Slemr, J., Schlager, H., Schulte, P., Haschberger,
 485 P., Lindermeir, E., Döpelheuer, A., & Plohr, M. (2001). In-flight measurement of aircraft CO and nonmethane
 486 hydrocarbon emission indices. *J. Geophys. Res.: Atmos.*, 106(D7), 7485–7494.
- 487 (Spicer et al., 1994) Spicer, C., Holdren, M., Riggin, R., & Lyon, T. (1994). Chemical composition and
 488 photochemical reactivity of exhaust from aircraft turbine engines. In *Ann. Geophys.*, 12, 944–955.
- 489 (Tkacik et al., 2012) Tkacik, D. S., Presto, A. A., Donahue, N. M., & Robinson, A. L. (2012). Secondary
 490 organic aerosol formation from intermediate-volatility organic compounds: cyclic, linear, and branched alkanes.
 491 *Environ. Sci. Technol.*, 46(16), 8773–8781.
- 492 (Unal et al., 2005) Unal, A., Hu, Y., Chang, M. E., Odman, M. T., & Russell, A. G. (2005). Airport
 493 related emissions and impacts on air quality: Application to the Atlanta International Airport. *Atmos. Environ.*,
 494 39(32), 5787 – 5798.
- 495 (Westerdahl et al., 2008) Westerdahl, D., Fruin, S. A., Fine, P. L., & Sioutas, C. (2008). The Los Angeles
 496 International Airport as a source of ultrafine particles and other pollutants to nearby communities. *Atmos.*
 497 *Environ.*, 42(13), 3143–3155.
- 498 (Yee et al., 2013) Yee, L., Kautzman, K., Loza, C., Schilling, K., Coggon, M., Chhabra, P., Chan, M.,
 499 Chan, A., Hersey, S., Crouse, J., et al. (2013). Secondary organic aerosol formation from biomass burning
 500 intermediates: phenol and methoxyphenols. *Atmos. Chem. Phys.*, 13(16), 8019–8043.

501

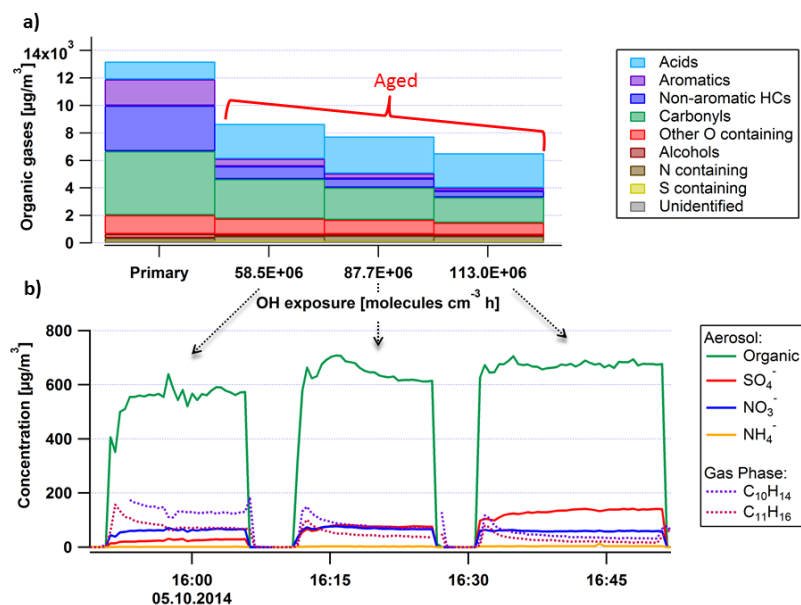
502



503

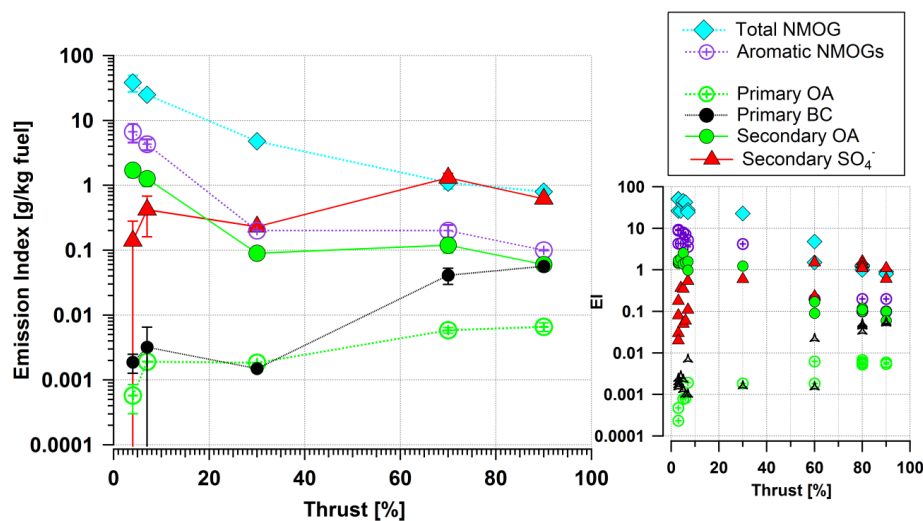
504

Figure 1: Simplified scheme of the experimental setup.



505
 506
 507
 508
 509
 510
 511

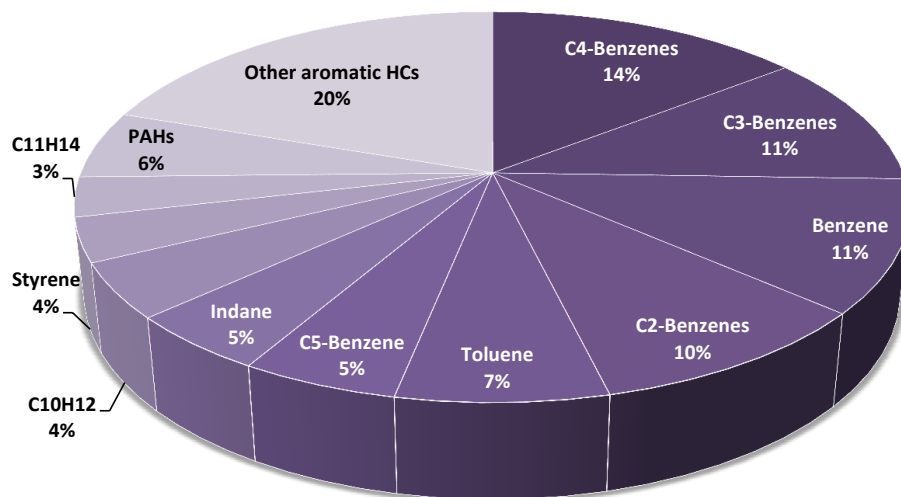
Figure 2: Sample experiment showing mean NMOG emissions (top) and representative time series for particle and NMOG components (bottom) for varying OH exposures. Hydrocarbon concentrations (non-aromatic HCs (dark blue), aromatic HCs (purple) and carbonyls (green) decrease in the PAM while the concentrations of acids (mostly formic and acetic ~90% of the total acids) increase. The bottom panel shows the aerosol (Organic, SO_4^- , NO_3^- , NH_4^+) formed and gaseous aromatics ($\text{C}_{10}\text{H}_{14}$, $\text{C}_{11}\text{H}_{16}$) for the different OH exposures in the PAM given in the top panel.



512
 513
 514
 515
 516
 517

Figure 3: Average emission indices (left) and EIs from individual test points (right) for primary non-methane organic gases (NMOGs), aromatic gases, primary organic aerosol (POA), equivalent black carbon (BC), secondary organic aerosol (SOA), nitrate (NO_3^-) and sulfate (SO_4^-). Error bars (+/-) are the standard deviations of the means with a confidence interval of 95%. The OH exposure was in the range of $91\text{--}113 \times 10^6$ molecule cm^{-3} h for the secondary aerosol cases.

518
 519



520

521

522

523

Figure 4: Mass fractions of aromatic compounds for primary emissions (directly emitted) at idle (thrust 3-7%). Benzene derivatives, xylenes, tri-, tetra-, pentamethylbenzene, benzene and toluene account for ~60% of all aromatics.

524

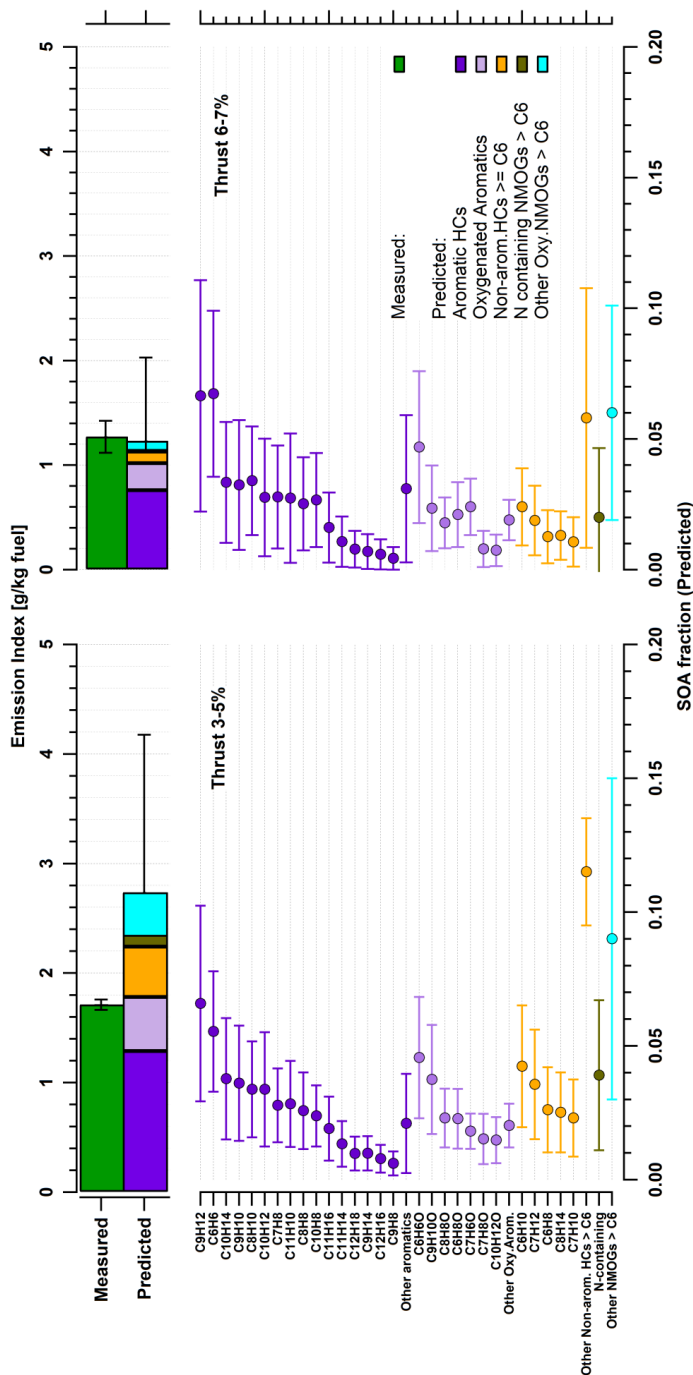


Figure 5: Comparison of the SOA measured by the AMS and the SOA predicted by the oxidation of NMOGs (top panel). The statistics are presented for low load idling (thrust 3-5%) on the left half and for idling 6-7% on the right. Aromatic hydrocarbons (purple) were the most abundant precursors of SOA at idle (thrust 3-7%) explaining all SOA formed (green, top panel) at thrust 3-5% and most (~90%) at thrust 6-7%. Aromatic SOA comprised the largest fraction followed by oxygenated aromatics (light purple - e.g. phenol, benzaldehydes), non-aromatic hydrocarbons (orange) with more than 6 carbon atoms in their molecular structure (non-arom. HCs \geq C6), nitrogen containing compounds (brown), other oxygenated-NMOGs $>$ C6 (cyan). Average fractions of individual NMOGs (bottom panel) were calculated by using SOA yields from literature (see Table 2) and the amount of NMOG reacted. Error bars show standard deviations of the means (CI: 95%).

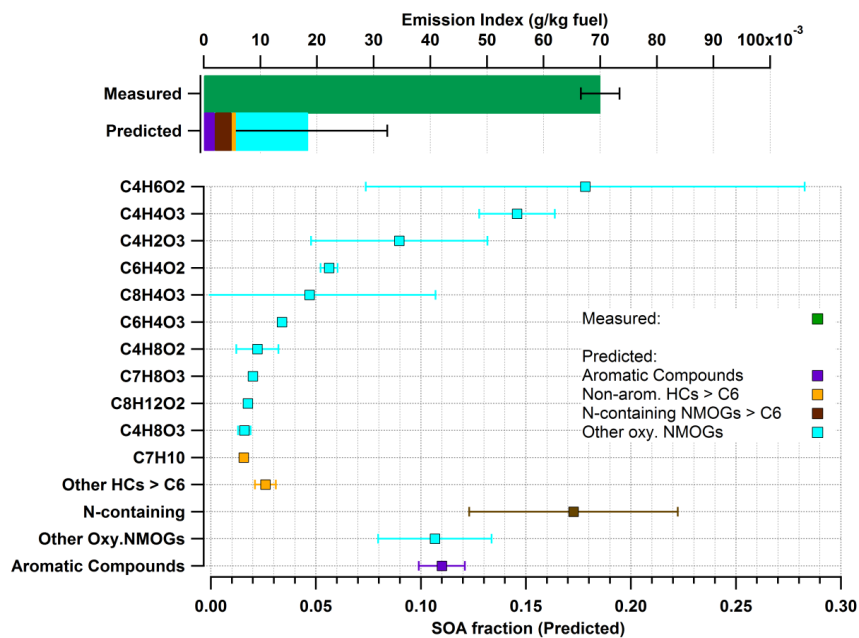


Figure 6: Measured and predicted SOA comparison at an approximated cruise load, using the same approach as in Fig. 5. In contrast to idle conditions, total NMOGs detected do not explain SOA formed.



Table 1: Volume mixing ratios of gaseous emissions, engine parameters and emission indices (EIs) for primary (directly emitted) and secondary (after aging) for all experiments.

Thrust (%)	Fuel Consumption (kg/sec)	Primary							Aged			
		CO ₂ (ppmv)	CO (ppmv)	THC (ppmvC)	NO _x (ppmv)	NMOC (g/kg fuel)	Aromatic Gases (g/kg fuel)	BC (g/kg fuel)	POA (g/kg fuel)	SO ₄ (g/kg fuel)	OH exposure (molec. cm ⁻³ h)	SOA (g/kg fuel)
3	0.09	1863	764	239	14	51	9.4	1.70E-06	2.34E-04	0.03	8.80E+07	1.4
3	0.09	1831	766	244	14	51	8.8	2.00E-06	4.74E-04	0.02	8.80E+07	n/a
3	0.09	1560	709	222	14	26	4.3	1.50E-06	<2.0E-03	0.08	6.00E+07	1.5
3	0.09	1560	709	222	14	26	4.3	2.40E-06	<2.0E-03	0.18	9.00E+07	1.7
3	0.09	1560	709	222	14	26	4.3	2.80E-06	<2.0E-03	0.37	1.13E+08	1.9
4	n/a	1884	543	173	n/a	39	7.7	2.30E-06	<2.0E-03	0.35	1.00E+08	2.6
5	0.11	1829	442	114	17	46	7.9	1.30E-06	7.81E-04	0.05	8.80E+07	1.4
5	0.11	1758	422	98	17	42	7.1	1.00E-06	8.13E-04	0.06	8.80E+07	1.5
6	0.12	1934	410	113	21	28	5.2	1.00E-06	<2.0E-03	0.54	1.00E+08	1.6
7	0.14	1909	168	45	23	25	3.6	7.00E-06	1.91E-03	0.11	8.80E+07	1.0
7	0.14	1978	385	94	23	23	4.2	1.60E-06	<2.0E-03	0.6	1.00E+08	1.2
30	0.31	2953	40	8	62	5	0.2	1.50E-06	1.84E-03	0.23	8.80E+07	0.1
60	0.65	3709	12	7	131	2	0.2	2.20E-05	6.21E-03	1.51	8.50E+07	0.2
60	0.65	3709	12	7	131	1	0.2	3.30E-05	6.80E-03	1.61	8.50E+07	0.1
80	0.9	4344	16	6	195	1	0.1	4.60E-05	5.55E-03	1.39	1.00E+08	0.1
80	0.9	4291	14	7	195	1	0.2	4.40E-05	6.01E-03	1.16	8.50E+07	0.1
80	0.9	4291	14	7	195	1	0.2	5.00E-05	5.24E-03	1.1	8.50E+07	0.1
80	0.9	4291	14	7	195	1	0.2	5.20E-05	5.37E-03	1.1	8.50E+07	0.1
90	1.1	4657	16	6	202	1	0.1	5.50E-05	5.89E-03	0.61	8.50E+07	0.1
90	1.1	4657	16	6	202	1	0.1	5.80E-05	7.30E-03	0.63	8.50E+07	0.1



Table 2. Precursor OGs, their corresponding functional group and protonated m/z, SOA yield coefficients* from literature, and average SOA EI estimated for different thrusts.

VOC formula	m/z	Group	SOA yield*	SOA Emission Index (g/kg fuel)			
				Thrust 3-5%		Thrust 6-7%	
				Average	±	Average	±
(C ₉ H ₁₂)H ⁺	121.101	Aromatic	0.32	0.19	0.11	0.07	0.04
(C ₆ H ₆)H ⁺	79.054	Aromatic	0.33	0.16	0.06	0.07	0.03
(C ₁₀ H ₁₄)H ⁺	135.117	Aromatic	0.2	0.11	0.07	0.03	0.02
(C ₉ H ₁₀)H ⁺	119.086	Aromatic	0.32	0.10	0.06	0.03	0.02
(C ₈ H ₁₀)H ⁺	107.086	Aromatic	0.2	0.10	0.05	0.04	0.02
(C ₁₀ H ₁₂)H ⁺	133.101	Aromatic	0.32	0.10	0.06	0.03	0.02
(C ₇ H ₈)H ⁺	93.070	Aromatic	0.24	0.08	0.04	0.03	0.02
(C ₁₁ H ₁₀)H ⁺	143.086	Aromatic	0.52	0.08	0.05	0.03	0.02
(C ₈ H ₈)H ⁺	105.070	Aromatic	0.32	0.07	0.04	0.03	0.02
(C ₁₀ H ₈)H ⁺	129.070	Aromatic	0.52	0.07	0.03	0.03	0.02
(C ₁₁ H ₁₆)H ⁺	149.132	Aromatic	0.2	0.05	0.03	0.02	0.01
(C ₁₁ H ₁₄)H ⁺	147.117	Aromatic	0.2	0.04	0.02	0.01	0.01
(C ₁₂ H ₁₈)H ⁺	163.148	Aromatic	0.2	0.03	0.02	0.01	0.01
(C ₉ H ₁₄)H ⁺	123.117	Aromatic	0.2	0.03	0.02	0.01	0.01
(C ₁₂ H ₁₆)H ⁺	161.132	Aromatic	0.2	0.02	0.01	0.01	0.01
(C ₉ H ₈)H ⁺	117.070	Aromatic	0.2	0.02	0.01	0.00	0.00
Other	-	Aromatic	0.2	0.06	0.05	0.00	0.00
(C ₆ H ₆ O)H ⁺	95.049	Oxy-arom	0.44	0.13	0.07	0.05	0.03
(C ₆ H ₈ O)H ⁺	97.065	Oxy-arom	0.32	0.07	0.03	0.02	0.01
(C ₇ H ₆ O)H ⁺	107.049	Oxy-arom	0.32	0.05	0.02	0.02	0.01
(C ₆ H ₆ O ₂)H ⁺	111.044	Oxy-arom	0.39	0.03	0.01	0.01	0.00
(C ₁₀ H ₁₂ O ₂)H ⁺	165.091	Oxy-arom	0.2	0.00	0.00	0.00	0.00
(C ₁₀ H ₁₄ O ₂)H ⁺	167.107	Oxy-arom	0.2	0.00	0.00	0.00	0.00
Other NMOGs	> 79.054	Other NMOG	0.15	1.15	0.74	0.20	0.02

*SOA yields from (Ng et al., 2007; Alvarez et al., 2009; Chan et al., 2009; 2010; Hildebrandt et al., 2009; Shakya and Griffin, 2010; Chhabra et al., 2011; Nakao et al., 2011; Yee et al., 2013)